

Dual representation for pure Yang-Mills SU(2) gauge theory

R. Leme,^{1,*} O. Oliveira,^{2,†} and G. Krein^{1,‡}

¹*Instituto de Física Teórica, Universidade Estadual Paulista,*

Rua Dr. Bento Teobaldo Ferraz, 271 - Bloco II, 01140-070 São Paulo, Brazil

²*CFisUC, Department of Physics, University of Coimbra, P-3004 516 Coimbra, Portugal*

A dual representation for non-Abelian lattice gauge theories where the new set of dynamical variables belong to the natural numbers \mathbb{N}_0 is discussed. After looking at the constraints on the dual variables due to gauge symmetry, the theory for the gauge group SU(2) is solved using Monte Carlo simulations based on Prokof'ev-Svistunov worm type of algorithms. The performance of the Monte Carlo is investigated for different types of updates. To test our approach the plaquette mean value is computed for a large range β values and compared to the results from a conventional heat bath method. We find that the worm approach to the dual representation is able to reproduce the heat bath numbers. Furthermore, the mass of the lightest $J^{PC} = 0^{++}$ glueball state is also evaluated and is in good agreement with the literature.

I. INTRODUCTION

The computation of hadron properties directly from Quantum Chromodynamics (QCD) is still challenging. For matter at zero baryon density, Monte Carlo lattice QCD simulations are currently used to address both zero and finite temperature [1]. On the other hand, to address the properties of dense quark matter, as required for example study the structure of atomic nuclei and neutron stars, the quark-gluon plasma produced in heavy ion collisions and the early stages of the history of the Universe, are, from the algorithmic point of view, open problems for lattice QCD simulations. Indeed, the investigation of such systems, e.g. in the grand canonical ensemble, demands the introduction of a finite chemical potential μ in the partition function of the theory. The baryon chemical potential turns the action into a complex-valued function and the integration measure in the path integral of the partition function is no longer positive definite, giving rise to the so-called sign problems, and thereby limits the use of Monte Carlo techniques with importance sampling. For sufficiently small values of μ , the study of dense systems can still rely on importance sampling when combined with re-weighting [2, 3]. However, in general, the handling of complex actions requires the introduction of new sampling techniques as, for example, the direct sampling of the density of states or a mapping of the theory into new variables such that one recovers a positive Boltzmann factor; in this latter approach, the theory reformulated in terms of the new variables is called the dual theory — Ref. [4] provides a recent review on these methods for lattice field theories. The mapping of a given theory into its dual has been used to overcome sign problems appearing in different fields [5].

In lattice QCD in the strong coupling limit, the sign problems can be avoided by mapping the theory into a

dual representation, using new “dual variables”, after the integration of the gauge fields prior to the integration of the fermion fields [6–8]. The gauge symmetry of the original theory imposes constraints on the dual variables which, nevertheless, can be handled via generalizations of the original Prokof'ev-Svistunov worm algorithm [9]. An additional feature of worm algorithms is that their dynamical critical exponents are close to zero and, therefore, they do not suffer from the problem of critical slowing down.

Another example of a dual representation of QCD is the effective theory introduced in Ref. [10], where the fundamental degrees of freedom are the Polyakov loops defined in the group $\mathbb{Z}(3)$. This effective theory can be derived from QCD by taking the strong coupling limit, by restricting the non-Abelian gauge degrees of freedom to the center of the group SU(3), i.e. to the group $\mathbb{Z}(3)$, and performing a hopping expansion in the quark sector. The action of the $\mathbb{Z}(3)$ effective theory inherits a sign problem from QCD. However, after rewriting the original partition function in terms of dual variables, it becomes a sum of real and positive Boltzmann weights [11]. The dual variables are *dimers*, that are attached to the lattice links, and *monomers*, that are attached to the lattice sites. In the dual representation, the complex nature of the original action given in terms of Polyakov loops is washed out [11]. Symmetries of the original theory appear, again, as constraints on the dual variables in the reformulated theory that can be handled with the use of a worm algorithm.

In recent years several other interesting QCD related theories were studied using its dual representations. Theories with O(N) and CP(N-1) symmetries, which, like QCD, are asymptotically free, were investigated with worm algorithms at zero [12, 13] and finite density [14]. Strongly interacting fermionic theories, relevant for graphene [15] and also for particle physics, were investigated with the fermion bag approach [16–19], in which a dual representation can be built after a suitable integration of the fermionic degrees of freedom which are responsible for sign problems. Then, by combining strong coupling and hopping parameter expansions one can ar-

* rleme@ift.unesp.br

† orlando@teor.fis.uc.br

‡ gkrein@ift.unesp.br

rive at an effective theory [20] where the dual representation, formulated in a way suitable to use the worm algorithm approach, is free of sign problems. Scalar field theories have also been successfully mapped into dual representations suitable for the implementation of worm algorithms, see, e.g. Refs. [21–25].

In what concerns gauge field theories, a worm-based dual representation was implemented for pure Abelian $U(1)$ theory in Ref. [26, 27], Higgs- $U(1)$ theory in Ref. [28, 29], and $U(1)$ Abelian theory with fermion fields in Ref. [30]. Recently, a dual representation for non-Abelian gauge theories was suggested in Ref. [31]. However, the partition function for the dual theory is given by a sum of positive and negative terms, which prevents the use of Monte Carlo simulations with importance sampling to solve the theory.

In the current work we discuss a new dual representation for pure non-Abelian gauge theories suitable to implement a Metropolis-type worm-based algorithm. Explicit numerical results are presented for the $SU(2)$ gauge group. Starting from the partition function written in terms of the Wilson action, we expand the exponential of a single plaquette as a power series and associate to each plaquette a positive natural number $b_{\mu\nu}(x) \in \mathbb{N}_0$ that, after integrating over the gauge fields, plays the role of a dynamical variable. The Boltzmann weights become functions of the dual variables $b_{\mu\nu}(x)$, and a Metropolis-type worm-based algorithm can be built, where the transition probabilities of the corresponding Markov chain are ratios between these weights. In the new representation of the non-Abelian gauge theory, the weights are computed by integrating the link variables. In the dual theory, the integration over the links is a non-trivial problem *per se* as each link is coupled to all of the links in the entire lattice. For the numerical experiment, we make approximations in the integration over the link fields to estimate the transition probability defining the Markov chain and thus generate ensembles of the dual variables $\{b_{\mu\nu}(x)\}$.

In this work we investigate only the pure Yang-Mills gauge theory associated to the gauge group $SU(2)$. The boson sector of a gauge theory does not suffer from the sign problem but it is a first setep towards the simulation of the full theory. We plan to extend our results by including matter fields in the future. The rationale, see below, to build a dual representation can, in principle, be extended to the fermionic sector. The full theory requires using an enlarged set of dynamical variables, defined after the expansion of the terms appearing in the action. Further, for full QCD the constraints in the dual theory due to the gauge symmetry are of the same type as those found for the pure Yang-Mills theory. On the other hand, the integration over the link fields requires a new analysis.

We test our algorithm by computing the plaquette mean value, related to the energy density of the pure gauge system, over a large range of the lattice β coupling constant and the mass of the (expected) lighter scalar

glueball state ($J^{PC} = 0^{++}$). Our results show that the plaquette mean value for the worm algorithm deviates by less than 0.1% when compared with a standard heat bath simulation for $\beta \in [0, 4.5]$. The mass of lightest glueball agrees well with previous lattice estimates [32–38] and also with estimates based on a gauge-gravity duality model [39].

Our paper is organized as follows. In the next section we present our dual representation for the non-Abelian Yang-Mills theory. In Sec. III we discuss the constraints on the dual variables due to gauge symmetry which determines the types of updates that we should consider in a worm algorithm approach to solve the theory. In Sec. IV we discuss the algorithm used in Monte Carlo simulations of Yang-Mills theories in the dual representation and, in particular, strategies to decouple a region from the entire lattice surrounding a dual variable to be updated locally. In the factorized region, the group integrals are done analytically. Still in Sec. IV we show how to implement one possible type of nonlocal update. In Sec. V we present how to write the observables to be measured in the dual representation. In Sec. VI we show details of the simulations and report the numerical data for the observables of the previously discussed. A summary in Sec. VII completes the paper.

II. DUAL REPRESENTATION FOR LATTICE YANG-MILLS THEORY

The lattice formulation of pure Yang-Mills theory uses as fundamental fields the link variables $U_\mu(x)$, which belong to the gauge group $SU(N)$. We consider the standard Wilson action [40]:

$$S[U] = \frac{\beta}{N} \sum_{x \in V} \sum_{\mu < \nu} \text{Re Tr} [\mathbb{1} - U_{\mu\nu}(x)], \quad (1)$$

with the plaquette $U_{\mu\nu}(x)$ given by the product of link variables

$$U_{\mu\nu}(x) = U_\mu(x) U_\nu(x + \hat{\mu}) U_\mu^\dagger(x + \hat{\nu}) U_\nu^\dagger(x), \quad (2)$$

where the spacetime indices μ and ν run from 1 to d , with d being the dimension of the Euclidean space, and x runs over the lattice volume V . The partition function of the theory is given by

$$Z = C \int \mathcal{D}U \prod_{x, \mu < \nu} e^{\frac{\beta}{N} \text{Re Tr}[U_{\mu\nu}(x)]}, \quad (3)$$

where $C = \exp(-\beta N V_p^{-1})$ is a normalisation factor, V_p is the number of plaquettes in the volume V and $\mathcal{D}U = \prod_{x, \mu} dU_\mu(x)$ is the Haar measure for the gauge links. Given an operator $\mathcal{O}(U)$, its vacuum expectation value is represented by the functional integral

$$\langle \mathcal{O} \rangle = \frac{C}{Z} \int \mathcal{D}U \prod_{x, \mu < \nu} e^{\frac{\beta}{N} \text{Re Tr}[U_{\mu\nu}(x)]} \mathcal{O}(U). \quad (4)$$

In the traditional lattice approach, this expectation value is estimated by the average

$$\langle \mathcal{O} \rangle \approx \frac{1}{N_{conf}} \sum_{i=1}^{N_{conf}} \mathcal{O}(U^{(i)}) \quad (5)$$

where the set of configurations $\mathcal{U} = \{U^{(i)}, i = 1, \dots, N_{conf}\}$, distributed according $\exp\{-S[U]\}$, is generated with a Monte Carlo algorithm. The statistical error associated with such an estimate scales with the number of configurations as $1/\sqrt{N_{conf}}$.

The simulation of Yang-Mills theory with a worm algorithm demands rewriting the partition function in Eq. (3) in terms of a new set of dynamical variables other than the links. In order to be able to apply such a type of algorithm, let us expand the exponentials appearing in the partition function in powers of β

$$Z = \int \mathcal{D}U \prod_{x, \mu < \nu} \sum_{b_{\mu\nu}(x)} \frac{1}{[b_{\mu\nu}(x)]!} \times \left(\frac{\beta}{N} \text{Re Tr } U_{\mu\nu}(x) \right)^{b_{\mu\nu}(x)}, \quad (6)$$

where we have discarded for the moment the global factor C . Performing the integration over the link variables, i.e. computing the integral $\int \mathcal{D}U$, Z can then be viewed as a function of the discrete set of variables $b_{\mu\nu}(x)$, which are natural numbers. Let us introduce the notation

$$\sum_{\{b\}} = \prod_{x, \mu < \nu} \sum_{b_{\mu\nu}(x)}, \quad (7)$$

so that the partition function can be written as

$$Z = \sum_{\{b\}} Q_{\{U\}}[\{b\}], \quad (8)$$

where

$$Q_{\{U\}}[\{b\}] = \int \mathcal{D}U \prod_{x, \mu < \nu} \left(\frac{\beta}{N} \right)^{b_{\mu\nu}(x)} \times \frac{1}{[b_{\mu\nu}(x)]!} [\text{Re Tr } U_{\mu\nu}(x)]^{b_{\mu\nu}(x)}. \quad (9)$$

The integration of the link variables defines the weights $Q_{\{U\}}[\{b\}]$ which are, themselves, functions of the natural numbers $b_{\mu\nu}(x)$, the new dynamical variables called from now on plaquette occupation number (PON). Then, one can define a Markov chain to update the $b_{\mu\nu}(x)$ values by choosing a transition probability given by the ratio of the weight functions $Q_{\{U\}}[\{b\}]$, that complies with the principle of detailed balance and ensures the convergence of the Markov chain to the right probability distribution. Before dealing with the details of the update, let us discuss the constraints on $b_{\mu\nu}(x)$ due to the group integration over the link variables.

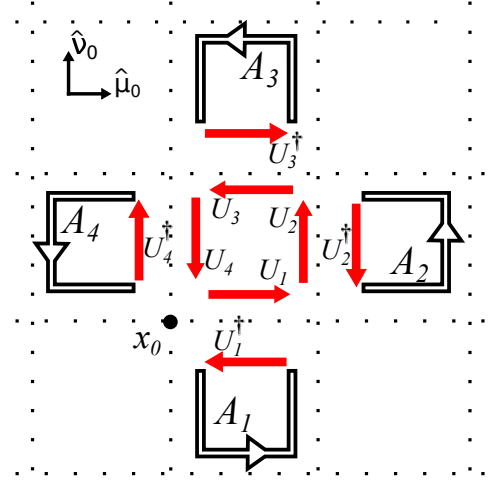


FIG. 1. Representation of the (μ_0, ν_0) lattice plane. The gauge links are shown as arrows. The “central plaquette” $U_{\mu_0\nu_0}(x_0) = U_1 U_2 U_3 U_4$ (in solid red arrows) and the plaquettes which contain any of the links appearing in $U_{\mu_0\nu_0}(x_0)$. A_i are the staples (in non-solid black lines), defined in the (μ_0, ν_0) plane, required to complete the neighboring plaquettes besides the links in the “central plaquette”.

III. CONSTRAINTS ON THE DUAL VARIABLES $b_{\mu\nu}(x)$

In this section, we discuss the constraints on $b_{\mu\nu}(x)$ due to the group integration over the gauge links. The results and the group integrations discussed below can, in principle, be extended to $SU(N)$ but herein we restrict our analysis to the gauge group $SU(2)$. The main properties and results for the group integration required to understand the current work are summarized in the Appendix A.

Let us consider the plaquette

$$U_{\mu_0\nu_0}(x_0) = U_{\mu_0}(x_0) U_{\nu_0}(x_0 + \hat{\mu}_0) U_{\mu_0}^\dagger(x_0 + \hat{\nu}_0) U_{\nu_0}^\dagger(x_0) = U_1 U_2 U_3 U_4, \quad (10)$$

defined on the (μ_0, ν_0) plane, see Fig. 1 where U_l with $l = 1, \dots, 4$ stands for a generic link and l is a composite index taking values in the set:

$$L = \{(x_0, \mu_0); (x_0 + \hat{\mu}_0, \nu_0); (x_0 + \hat{\nu}_0, \mu_0); (x_0, \nu_0)\}. \quad (11)$$

Let A_i be the staple that together with the link variable U_i defines a plaquette in the (μ_0, ν_0) plane which shares with $U_{\mu_0\nu_0}(x_0)$ the link U_i — see Fig. 1. In the following, to simplify the notation, we will write b_l for the dynamical variable that is associated with the plaquette containing the staple A_l , i.e. the staple in the plane (μ_0, ν_0) that is associated with the link U_l . The weight function Q associated with the plaquettes repre-

sented on Fig. 1 is

$$\begin{aligned}
Q_{\{U\}}[\{b\}] &= \left(\frac{\beta}{N}\right)^{\sum b_{\mu\nu}(x)} \int \mathcal{D}U \\
&\times \frac{1}{b_0!} [\text{Tr } U_1 U_2 U_3 U_4]^{b_0} \\
&\times \frac{[\text{Tr } U_1 A_1^\dagger]^{b_1}}{b_1!} \times \frac{[\text{Tr } U_2 A_2^\dagger]^{b_2}}{b_2!} \\
&\times \frac{[\text{Tr } U_3 A_3^\dagger]^{b_3}}{b_3!} \times \frac{[\text{Tr } U_4 A_4^\dagger]^{b_4}}{b_4!} \dots \quad (12)
\end{aligned}$$

The properties of the group integration are such that most of the possible sets $\{b\}$ have a null weight and do not contribute to the partition function. The non-vanishing contributions are those where a given link variable U_l , with $l = (\mu, x)$, appears n_l times in the integrand, with n_l being a multiple of N , where N is the number of colors. Consider, for example, the link variable U_2 in Eq. (12): it appears $b_0 + b_2 = n_2$ times in the integrand, i.e.

$$\int dU_2 (U_2)_{i_1 j_1} (U_2)_{i_2 j_2} \dots (U_2)_{i_{n_2} j_{n_2}}, \quad (13)$$

and this gives a non-vanishing contribution to $Q_{\{U\}}[\{b\}]$ only if $n_2 = b_0 + b_2$ is a multiple of N . This implies that b_0 and b_2 are either multiples of N or their sum is a multiple of N , despite $(b_0 \bmod N) \neq 0$ and $(b_2 \bmod N) \neq 0$. In four dimensions, the link U_2 belongs to the plaquettes represented in Fig. 1 and also to plaquettes belonging to orthogonal planes not shown in the figure. Therefore, for a generic link $U_\mu(x)$, it follows that the sum over the set $\{b_{\mu\nu}(x)\}$ that count the number of times $U_\mu(x)$ appears in the integral in Eq. (12) is given by

$$\begin{aligned}
n_\mu(x) &= \sum_{\nu=1}^{\mu-1} [b_{\nu\mu}(x) + b_{\nu\mu}(x - \hat{\nu})] \\
&+ \sum_{\nu=\mu+1}^d [b_{\mu\nu}(x) + b_{\mu\nu}(x - \hat{\nu})], \quad (14)
\end{aligned}$$

and only those $\{b_{\mu\nu}(x)\}$ configurations such that all $\{n_\mu(x)\}$ are multiples of N contribute to the partition function, i.e.

$$n_\mu(x) \bmod N = 0. \quad (15)$$

This is a non trivial constraint that also simplifies the analysis of the possible sets of updates that can be associated with a Markov chain.

IV. UPDATE ALGORITHM

A possible local update compatible with Eq. (15) replaces $b_{\mu\nu}(x) \rightarrow b_{\mu\nu}(x) \pm \Delta$, with Δ being a multiple of N . In this way, if the original configuration $\{b_{\mu\nu}(x)\}$ verifies the constraint in Eq. (15), the new configuration

is also compatible with Eq. (15). On the other hand, if $(\Delta \bmod N) \neq 0$, then to fulfil Eq. (15) at all lattice points, one has to change the b values in the neighbouring points accordingly and, therefore, in the next neighbouring points and so on and so forth. The updates where Δ is not an integer multiple of N requires a global update over a finite region of the lattice.

An ergodic algorithm must access all possible b values and, therefore, requires the use of both local and nonlocal updates. If, for example, the Markov chain is initiated setting all PON such that $(b_{\mu\nu}(x) \bmod N) = 0$ and only local updates are implemented, i.e. a given b is modified by adding an integer multiple of N , configurations where all PONs of a given plane are not multiples of N cannot be reached and, therefore, the update does not verify the ergodicity requirement.

To ensure convergence to the right probability distribution, one needs to set a detailed balance equation compatible with Eq. (15). Our implementation choses randomly a b or a set of b 's and proposes new values b' . As usual in these types of algorithms, the transition probability for accepting the new b' is given by

$$p = \frac{P_{\{b\}^{\text{old}} \rightarrow \{b\}^{\text{new}}}}{P_{\{b\}^{\text{new}} \rightarrow \{b\}^{\text{old}}}} = \frac{Q[\{b\}^{\text{new}}]}{Q[\{b\}^{\text{old}}]}, \quad (16)$$

which is enough to ensure that the sampling reproduces the correct distribution probability [41].

The computation of the weights Q imply integration over the link variables, for all possible PONs configurations, defines a formidable problem. The Haar measure for the group integration is invariant under gauge transformations and this allows rotating the links and, eventually, replace some of them by the identity in the evaluation of the $Q[\{b\}]$ functions. In particular, a path in which the maximal number of links allowed by the group integration are rotated to the identity defines what is known as a “maximal tree” [42]. Our proposal consists in performing link integrations by considering a number of patches on the lattice, in that some of the “distant” links, relative to the sublattice, are replaced by the identity matrix. The replacement of a small subset of link variables by the identity matrix is clearly an approximation, but it enables to perform group integrations analytically.

From now on we will use the term “worm algorithm” for our update scheme. Strictly, the variables to be updated $b_{\mu\nu}(x)$ do not represent worldlines (worms) but rather they represent worldsheets. The worm algorithms for Yang-Mills theories that can be found in the literature, the sampling is established considering the strong coupling limit in the lowest order approximation [6, 7]. An advantage of our method is that it does not rely on the strong coupling limit.

A. Local update

To introduce the ideas behind our update scheme, let us start considering the crudest approximation possible

in the local update of a given plaquette occupation number, say $b_{\mu_0\nu_0}(x_0)$, associated with the central plaquette represented on Fig. 1, i.e. replace all the staples that are connected with $U_{\nu_0}(x_0)$ (the link U_4 on the figure) by the identity. Then, the integration over $U_{\nu_0}(x_0)$ is decoupled from the integrations over the remaining links, and

$$\begin{aligned} Q[\{b\}] &\approx \int dU_{\nu_0}(x_0) [\text{Tr } U_{\nu_0}(x_0)]^{n_0} Q'[\{b\}'] \\ &= Q'[\{b\}'] \int dU_{\nu_0}(x_0) [\text{Tr } U_{\nu_0}(x_0)]^{n_0}, \end{aligned} \quad (17)$$

where $n_0 = n_{\nu_0}(x_0)$ is calculated from Eq. (14), and $Q'[\{b\}']$ is independent of the link $U_{\nu_0}(x_0)$. In this way, the transition probability of the local update of the PON $b_0 = b_{\mu_0\nu_0}(x_0)$ is

$$\begin{aligned} p &= \frac{Q[\{b\}^{\text{new}}]}{Q[\{b\}^{\text{old}}]} \\ &\approx \frac{Q'[\{b'\}]}{Q'[\{b'\}]} \frac{\int dU_{\nu_0}(x_0) [\text{Tr } U_{\nu_0}(x_0)]^{n_0(\text{new})}}{\int dU_{\nu_0}(x_0) [\text{Tr } U_{\nu_0}(x_0)]^{n_0(\text{old})}} \\ &= \left(\frac{\beta}{N}\right)^{b_0} \frac{1}{b_0!} \frac{\int dU_{\nu_0}(x_0) [\text{Tr } U_{\nu_0}(x_0)]^{n_0(\text{new})}}{\int dU_{\nu_0}(x_0) [\text{Tr } U_{\nu_0}(x_0)]^{n_0(\text{old})}}. \end{aligned} \quad (18)$$

To improve on the estimation of p , couplings of $U_{\nu_0}(x_0)$ to neighboring links need to be considered. A possible next level of approximation is to set all the staples associated with $U_{\nu_0}(x_0)$ to the identity with exception of $g = U_1 U_2 U_3$ (see Fig. 1), then

$$Q[\{b\}] \approx Q''[\{b\}'] \int dU_{\nu_0}(x_0) F[U_{\nu_0}(x_0), g], \quad (19)$$

where

$$F[U_{\nu_0}(x_0), g] = [\text{Tr } U_{\nu_0}^\dagger(x_0)]^{n_0-b_0} [\text{Tr } U_{\nu_0}(x_0)g]^{b_0}, \quad (20)$$

and $Q''[\{b\}']$ is the group integral over all the lattice links except for $U_{\nu_0}(x_0)$. Now, since $Q''[\{b\}']$ and the integral in Eq. (19) share the links U_1 , U_2 , and U_3 they do not decouple and this would not allow us to obtain a number for the transition probability p . However, as we shall discuss in the next two subsections, one can still devise a strategy that allows us to integrate over $U_{\nu_0}(x_0)$ taking into account couplings with neighboring links, so that under a local update $b_0^{\text{old}} \rightarrow b_0^{\text{new}}$, the transition probability is the positive real number given by

$$p = \frac{Q[\{b\}^{\text{new}}]}{Q[\{b\}^{\text{old}}]} \approx \frac{\int \widetilde{\mathcal{D}}U F[\mathcal{U}, \mathcal{B}, b_0^{\text{new}}]}{\int \widetilde{\mathcal{D}}U F[\mathcal{U}, \mathcal{B}, b_0^{\text{old}}]}, \quad (21)$$

where F contains through \mathcal{U} a subset of all links $U_\mu(x)$ of the lattice that are integrated, and \mathcal{B} stands for the PONs associated with the PON b_0 which is being updated.

The Monte Carlo updates considered in the present work approximate the weight functions Q following the type of approach discussed above. The integration of the

functions F considered in this work all give positive definite answers and, thus, the approximate ratio between the dual Boltzmann weights Q to estimate the transition probability p is also a positive real number. However, for the general case we have not been able to demonstrate the positivity of the dual weigh functions.

1. Integration over a short path

Let us consider Fig. 1 and the central plaquette associated with $b_0 = b_{\mu_0\nu_0}(x_0)$. The links belonging to this plaquette (solid red arrows) also contribute to the staples $A_i = \{A_1, A_2, A_3, A_4\}$ (non-solid black lines). Recall that the aim is to update b_0 and compute the transition probability p .

A maximal tree can be built by rotating some, but not all, staples associated with the links U_i in the plaquette $U_{\mu_0\nu_0}(x_0)$ to the identity matrix. However, assuming that all the links in A_i can be set to the identity, the group integration can be factorized and one has to consider only the following integrating function

$$\begin{aligned} F_4 &= F_4[\mathcal{U}, \mathcal{B}, b_0] \\ &= \frac{1}{b_0!} \left(\frac{\beta}{N}\right)^{b_0} \text{Tr}[U_1 U_2 U_3 U_4]^{b_0} \\ &\quad \times \text{Tr}[U_1^\dagger]^{c_1} \text{Tr}[U_2^\dagger]^{c_2} \text{Tr}[U_3^\dagger]^{c_3} \text{Tr}[U_4^\dagger]^{c_4}, \end{aligned} \quad (22)$$

with the integration measure given by

$$\widetilde{\mathcal{D}}U_4 = dU_1 dU_2 dU_3 dU_4. \quad (23)$$

The set $\mathcal{U} = \{U_1, U_2, U_3, U_4\}$ contains the link variables to be integrated. The set \mathcal{B} contains the PONs that couple the plaquette $U_{\mu_0\nu_0}(x_0)$ with the neighboring plaquettes and in two dimensions

$$\begin{aligned} \mathcal{B} &= \{b_{\mu_0\nu_0}(x_0 + \hat{\mu}_0), b_{\mu_0\nu_0}(x_0 - \hat{\mu}_0), b_{\mu_0\nu_0}(x_0 + \hat{\nu}_0), \\ &\quad b_{\mu_0\nu_0}(x_0 - \hat{\nu}_0)\}. \end{aligned} \quad (24)$$

For a generic dimensionality, the set \mathcal{B} contains the PONs that define the powers c_i in Eq. (22), i.e.

$$c_1 = n_{\mu_0}(x_0) - b_0, \quad (25)$$

$$c_2 = n_{\nu_0}(x_0 + \hat{\mu}_0) - b_0, \quad (26)$$

$$c_3 = n_{\mu_0}(x_0 + \hat{\nu}_0) - b_0, \quad (27)$$

$$c_4 = n_{\nu_0}(x_0) - b_0. \quad (28)$$

Let us now discuss the integration of F_4 with the measure $\widetilde{\mathcal{D}}U_4$ defined in Eq. (23). The integration over the links of the central plaquette can be started picking any of the links and for the function F_4 one can reduce the integration to

$$\begin{aligned} I_1[g; b, c] &= \int dU \text{Tr}[Ug]^b \text{Tr}[U^\dagger]^c \\ &= \left[\partial_x^b \partial_y^c \int dU e^{x \text{Tr}[Ug] + y \text{Tr}[U^\dagger]} \right]_{x=0, y=0}, \end{aligned} \quad (29)$$

where U and g are $SU(2)$ matrices. Integrals of this type have been computed in Ref. [43] and they are given by

$$I_1 = \left[\partial_x^b \partial_y^c \sum_{q=0}^{\infty} \frac{(xy \text{Tr}[g] + x^2 + y^2)^q}{q!(q+1)!} \right]_{\substack{x=0 \\ y=0}}. \quad (30)$$

For a non-vanishing result, the condition $2q = b + c$ must be fulfilled. The integral I_1 is a polynomial in $\text{Tr}[g]$, i.e.

$$I_1[g; b, c] = \sum_{q=0}^{\min(b, c)} \Gamma_q^{b, c} \text{Tr}[g]^q, \quad (31)$$

where $\min(b, c)$ stands for the minimum of b and c , the coefficients of the traces of g are given by

$$\Gamma_q^{b, c} = \delta_{\{q \% 2 \ b \% 2\}} \frac{b! \ c!}{\left(\frac{b+c}{2} + 1\right)! \left(\frac{b-q}{2}\right)! \left(\frac{c-q}{2}\right)! q!}, \quad (32)$$

and $\%2$ returns the remainder of the integer division by 2. The kronecker delta in Eq. (32) tells us that the polynomial (31) contains only odd or even powers. The evaluation of I_1 is a first step towards the evaluation of the weights Q . In our code the expression given in Eq. (31) was used directly. The routine to compute I_1 was checked against a numerical evaluation of I_1 for a number of cases and both results agreed within machine precision. The integral I_1 , given in Eq. (31), can be used recursively to perform the integration of Eq. (22):

$$\begin{aligned} \int \widetilde{\mathcal{D}U}_4 F_4 &= \left(\frac{\beta}{N}\right)^{b_0} \frac{1}{b_0!} \sum_{q_1}^{\min(b_0, c_1)} \Gamma_{q_1}^{b_0, c_1} \sum_{q_2}^{\min(q_1, c_2)} \Gamma_{q_2}^{q_1, c_2} \\ &\times \sum_{q_3}^{\min(q_2, c_3)} \Gamma_{q_3}^{q_2, c_3} \sum_{q_4}^{\min(q_3, c_4)} \Gamma_{q_4}^{q_3, c_4}. \end{aligned} \quad (33)$$

Once the coefficients $\Gamma_q^{b, c}$ are known, one can get an approximate estimation for the weights Q and also for the transition probability p which is defined in the Markov chain.

In principle, the calculation of the weights can be improved by considering more complex integrations over the gauge links as, for example:

$$\begin{aligned} I_2 &= \int dU \text{Tr}[Uv]^a [Ug]^b \text{Tr}[U^\dagger]^c \\ &= \left[\partial_x^a \partial_y^b \partial_z^c \sum_{q=0}^{\infty} \frac{1}{q!(q+1)!} (xy \text{Tr}[g^\dagger v] \right. \\ &\quad \left. + xz \text{Tr}[v] + yz \text{Tr}[g] + x^2 + y^2 + z^2)^q \right]_{\substack{x=0 \\ y=0 \\ z=0}}, \end{aligned} \quad (34)$$

However, the coding of this type of solutions in a Monte Carlo simulation is rather complex and will not be pursued here. Alternatively and keeping the same rationale as described so far, one can explore integrations over more complex paths on the lattice.

2. Integration over a long path

The method described in the previous section can be extended to more complex and longer lattice paths. From the practical point of view, one has to compromise the length and complexity of the path to perform the group integration with the coding of the outcome of group integration.

Herein, we consider an integration over the link variables which takes into account a larger set of links that are decoupled from the remaining lattice. On Fig. 2 we show, in color, the links to be integrated in the computation of the probability transition p . To avoid clutter, we do not draw all links to be integrated exactly. In particular, the links corresponding to the fourth dimension are not represented on the figure. For the path represented on Fig. 2, the links represented by solid red lines, which belong to the central plaquette $U_{\mu_0 \nu_0}(x_0)$, will be integrated exactly together with those represented by double blue lines and by triple green lines.

The links in double blue lines are in the same plane as $U_{\mu_0 \nu_0}(x_0)$ and their integration involves terms which include the links of the central plaquette. For example, the integrals referring to the links belonging to the plaquettes $U_{\mu_0 \nu_0}(x_0)$ and $U_{\mu_0 \nu_0}(x_2)$ are not independent as these staples share $U_{\mu_0}(x_2)$. The same applies to the links belonging to the plaquettes $U_{\mu_0 \nu_0}(x_0)$ and $U_{\mu_0 \nu_0}(x_4)$, whose staples share $U_{\mu_0}(x_3)$. Also, the integration over the links in the (μ, ν_0) plane are not independent of the integration of links in parallel planes as those represented by triple green lines. In our integration over the longer path, we will consider four green-type paths which belong to the upper parallel plane shown on Fig 2, on the down parallel plane and similar paths related to the path which dislocated not by $\hat{\rho}_0$ but by the unit vector belonging to the fourth dimension not represented on Fig 2. The later three paths are not represented on Fig 2.

In the computation of the weights Q and of the probability transition p the link variables represented in red (central plaquette with solid lines), blue (double lines) and green (triple lines) on Fig. 2 are integrated exactly. Each of these link variables is coupled with $2(d-1)$ staples which belong to $2(d-1)$ plaquettes. With the exception of the red, blue, and green links, all staples associated with the links which are going to be integrated are rotated to the identity matrix. On Fig. 2 the solid lines in gray represent the link variables that are being fixed to the identity matrix in the plane (μ_0, ν_0) . As in the integration described in Sec. IV A 1, we are not building a maximal tree. Indeed, there are closed paths whose links are all set to the identity. The approximation used to perform the group integrations factorizes a local region, which is decoupled from the remaining lattice, and, in this way, allows for an exact group integration in each of the regions considered. Furthermore, it factorises the calculation of the weights Q , which enables an easy estimation of the transition probability p .

Let us now discuss on how to integrate over the link

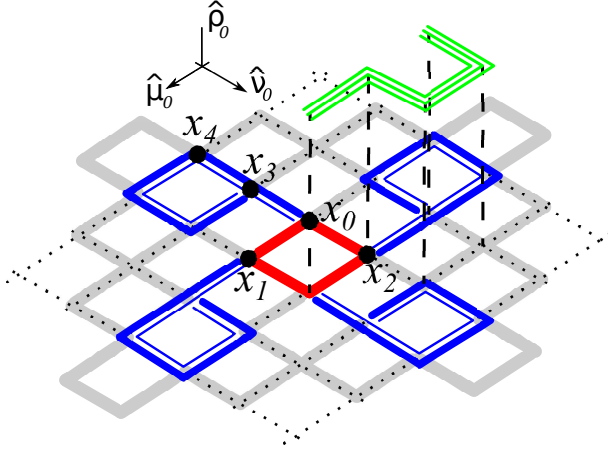


FIG. 2. A 3-dimensional representation of the lattice. For an update of the central plaquette $U_{\mu_0\nu_0}(x_0)$ (solid red lines), the links represented by red, blue (double lines) and green (triple lines) are integrated in the computation of the weight function ratio. In grey solid lines we shown a sample of the links that are rotated to the identity in the calculation of p . See text for details.

variables in color on Fig. 2. In principle one can choose to start the integration by considering any of the colored links. However, we found that starting the integration by the links in green or the links in blue and only then perform the integration of the links belonging to the central plaquette $U_{\mu_0\nu_0}(x_0)$ simplifies considerably the integration process. For the integration over a path that is coupled with the link $U_\mu(x)$ of the central plaquette, one can rely on the result given in Eq. (31) applied recursively. The outcome is a polynomial

$$P[U_\mu(x)] = \sum_k \lambda_k \text{Tr}[U_\mu(x)]^k, \quad (35)$$

whose coefficients λ_k are combinations of the coefficients Γ and are functions of the plaquette occupation numbers of the region surrounding the integrated path. For the group integration, every link belonging to the central plaquette is coupled with two different paths, namely, the path in green which has four links and the path in blue with five links. The total number of links to be integrated is now forty and for this larger integration we call $F_{40}[\mathcal{U}, \mathcal{B}, b_0]$ to the local function of the approximated weight function ratio, see Eq. (21). The set of links \mathcal{U} contains all the forty gauge links to be integrated and the set of the plaquette occupation numbers \mathcal{B} include the $b_{\mu\nu}(x)$ whose links are in the integrated paths. Recall that for the simpler integration discussed previously a similar situation is found.

The formal expression for $F_{40}[\mathcal{U}, \mathcal{B}, b_0]$ includes the central plaquette $U_{\mu_0\nu_0}(x_0)$ and four polynomials, one for each link variable $U_l \in U_{\mu_0\nu_0}(x_0)$, coming from the

integration over the green and blue paths

$$F_{40} = \frac{1}{b_0!} \left(\frac{\beta}{N} \right)^{b_0} \text{Tr}[U_1 U_2 U_3 U_4]^{b_0} \prod_{l \in L} P_{\mathcal{B}(l)}[U_l], \quad (36)$$

where L is the set of coordinates of the links associated with $U_{\mu_0\nu_0}(x_0)$, see Eq. (11). $P_{\mathcal{B}(l)}[U_l]$ is the polynomial coming from the integration of the green and blue paths coupled to the link variable U_l , i.e.

$$P_{\mathcal{B}(l)}[U_l] = P_{\mathcal{B}_G(l)}[U_l] P_{\mathcal{B}_B(l)}[U_l]. \quad (37)$$

The polynomial $P_{\mathcal{B}_G(l)}$ is the outcome of the integration over a green path and $P_{\mathcal{B}_B(l)}$ the outcome of integration over a blue path. The set $\mathcal{B}_G(l)$ includes the plaquette occupation numbers of the plaquettes whose links belong to the integrated green path. The set $\mathcal{B}_B(l)$ has the same meaning as $\mathcal{B}_G(l)$ but related to a blue path. The union of $\mathcal{B}_G(l)$ and $\mathcal{B}_B(l)$ defines the set $\mathcal{B}(l)$. Finally, the set \mathcal{B} , required to perform the group integration present in $F_{40}[\mathcal{U}, \mathcal{B}, b_0]$, is given by the union of the four sets $\mathcal{B}(l)$ together with the set of PONs of the plaquettes that share the links present in $U_{\mu_0\nu_0}(x_0)$.

Before providing expressions for $P_{\mathcal{B}_G(l)}$ and $P_{\mathcal{B}_B(l)}$ let us have a closer look on the integrations leading to these polynomials.

On Fig. 3 the green path coupled to the link U_3 is shown in full detail. This path has four links $\{U_{3a}, U_{3b}, U_{3c}, U_{3d}\}$ and the integration over these links gives

$$\begin{aligned} P_{\mathcal{B}_G}[U_3] &= \int \widetilde{\mathcal{D}}U_G \text{Tr}[U_3 U_{3d}]^{b_1} \text{Tr}[U_{3c} U_{3d}]^{b_2} \\ &\quad \times \text{Tr}[U_{3a} U_{3b} U_{3c}]^{b_3} \text{Tr}[U_{3a}]^{c_1} \\ &\quad \times \text{Tr}[U_{3b}]^{c_2} \text{Tr}[U_{3c}]^{c_3} \text{Tr}[U_{3d}]^{c_4}, \end{aligned} \quad (38)$$

and the integration measure reads

$$\widetilde{\mathcal{D}}U_G = dU_{3a} dU_{3b} dU_{3c} dU_{3d}. \quad (39)$$

The plaquette occupation numbers $\{b_1, b_2, b_3\}$ refer to the plaquettes $\text{Tr}[U_3 U_{3d}]$, $\text{Tr}[U_{3c} U_{3d}]$ and $\text{Tr}[U_{3a} U_{3b} U_{3c}]$, respectively, and $\{c_1, c_2, c_3, c_4\}$, i.e. the powers of the trace of the links that includes $\{U_{3a}, U_{3b}, U_{3c}, U_{3d}\}$, are given by sums of the plaquette occupation numbers similar to those found in the case discussed in Sec. IV A 1. For example, one has $c_1 = n_{x_0 + \hat{\nu}_0 + \hat{\rho} - \hat{\mu}_0, \nu_0} - b_3$. The definition of the remaining c_i and b_i associated with the integration over the green path is given in App. A.

The coefficients $\mathcal{B}_G = \{b_1, b_2, b_3, c_1, c_2, c_3, c_4\}$ take into account the coupling of the central plaquette and a green path attached to the link U_3 . The degree and the coefficients of the polynomial $P_{\mathcal{B}_G(l)}$ is determined by the values of the $\mathcal{B}_G(l)$.

The blue path associated with the link U_3 is shown on Fig. 4. The blue path associated with the link U_3 includes the plaquette occupation numbers associated with the first neighbor plaquette $\text{Tr}[U_3^\dagger \tilde{U}_{3e} \tilde{U}_{3d}^\dagger]$ of $U_{\mu_0\nu_0}(x_0)$

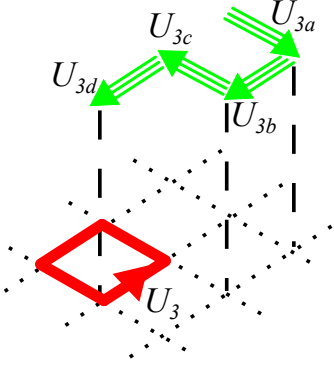


FIG. 3. Sublattice of the representation given on Fig. 2 with the links labeled.

and of its second neighbor $\text{Tr}[\tilde{U}_{3a}\tilde{U}_{3b}\tilde{U}_{3c}\tilde{U}_{3d}]$. The group integration over the blue path is

$$P_{B_B}[U_3] = \int \widetilde{\mathcal{D}}U_B \text{Tr} [\tilde{U}_{3a}\tilde{U}_{3b}\tilde{U}_{3c}\tilde{U}_{3d}]^{\tilde{b}_2} \times \text{Tr} [U_3^\dagger \tilde{U}_{3e} \tilde{U}_{3d}^\dagger]^{\tilde{b}_1} \text{Tr} [\tilde{U}_{3a}]^{\tilde{c}_1} \text{Tr} [\tilde{U}_{3b}]^{\tilde{c}_2} \times \text{Tr} [\tilde{U}_{3c}]^{\tilde{c}_3} \text{Tr} [\tilde{U}_{3d}]^{\tilde{c}_4} \text{Tr} [\tilde{U}_{3e}]^{\tilde{c}_5} \quad (40)$$

for an integration measure given by

$$\widetilde{\mathcal{D}}U_B = d\tilde{U}_{3a}d\tilde{U}_{3b}d\tilde{U}_{3c}d\tilde{U}_{3d}. \quad (41)$$

As for the green path, expressions for the coefficients \tilde{c}_i, \tilde{b}_i can be found in App. A.

The polynomials coming from performing the integrations over the green and blue paths are computed in App. A. It follows that for the green path

$$P_{B_G(l)}[U_l] = \sum_{q_1}^{\min(b_3, c_1)} \sum_{q_2}^{\min(q_1, c_2)} \sum_{q_3}^{\min(b_2, c_3 + q_2)} \times \sum_{q_4}^{\min(b_1, c_4 + q_3)} \Gamma_{q_1}^{b_3, c_1} \Gamma_{q_2}^{q_1, c_2} \Gamma_{q_3}^{b_2, c_3 + q_2} \times \Gamma_{q_4}^{b_1, c_4 + q_3} \text{Tr}[U_l]^{q_4}, \quad (42)$$

while the blue path the group integration gives

$$P_{B_B(l)}[U_l] = \sum_{\tilde{q}_1}^{\min(\tilde{b}_2, \tilde{c}_1)} \sum_{\tilde{q}_2}^{\min(\tilde{q}_1, \tilde{c}_2)} \sum_{\tilde{q}_3}^{\min(\tilde{q}_2, \tilde{c}_3)} \times \sum_{\tilde{q}_4}^{\min(\tilde{b}_1, \tilde{c}_4 + \tilde{q}_3)} \sum_{\tilde{q}_5}^{\min(\tilde{q}_4, \tilde{c}_5)} \Gamma_{\tilde{q}_1}^{\tilde{b}_2, \tilde{c}_1} \Gamma_{\tilde{q}_2}^{\tilde{q}_1, \tilde{c}_2} \times \Gamma_{\tilde{q}_3}^{\tilde{q}_2, \tilde{c}_3} \Gamma_{\tilde{q}_4}^{\tilde{b}_1, \tilde{c}_4 + \tilde{q}_3} \Gamma_{\tilde{q}_5}^{\tilde{q}_4, \tilde{c}_5} \text{Tr}[U_l]^{\tilde{q}_5}, \quad (43)$$

In order to evaluate Eq. (37) for each link of the central plaquette $U_l \in \{U_1, U_2, U_3, U_4\}$, it remains to multiply Eqs. (42) and (43). Once the polynomials $P_{B(l)}[U_l]$

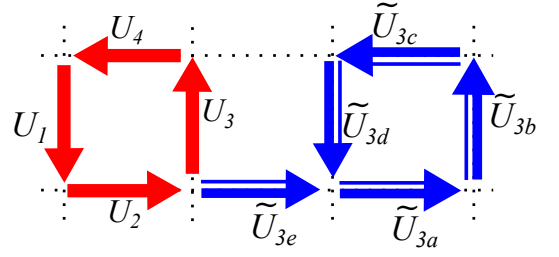


FIG. 4. Another sublattice of the representation given on Fig. 2 with the links labeled.

are known, we can integrate F_{40} , see Eq. (36), over the remaining links

$$\int \widetilde{\mathcal{D}}U_4 F_{40} = \int \widetilde{\mathcal{D}}U_4 \text{Tr}[U_1 U_2 U_3 U_4]^{b_0} \prod_{l \in L} P_{B(l)}[U_l], \quad (44)$$

and estimate the ratio between the weights Q in order to evaluate the probability transition p .

For the particular case of a local update transition $b_0 \rightarrow b_0 \pm \Delta$, the polynomials $P_{B(l)}[U_l]$ contributing to F_{40} do not depend on Δ , i.e. on the update of the central plaquette and, therefore, they do not need to be evaluated twice to compute p . Note that the function F_{40} defined in Eq. (36) is given by a sum of terms like F_4 given in Eq. (22). It follows that the solution of the group integration in Eq. (44) is a sum of the solutions that look like Eq. (33). Then, the group integration is reduced to the computation of factorial numbers and, it follows from the definition and the approximation used, that the transition probability is a real and positive definite number.

B. Nonlocal update

The Monte Carlo updates discussed in Secs. IV A, IV A 1 and IV A 2 do not allow us to access all possible configurations for the plaquette occupation numbers. For example, those local updates are unable to change a given plaquette occupation number from an odd natural number to an even natural number or vice-versa. As discussed in Sec. III, the introduction of a global or a nonlocal update can improve the algorithm in the sense that it enlarges the space sampled by the algorithm.

A nonlocal update can be implemented via a simultaneous transformation of all the plaquette occupation numbers over a plane surface, where each of the PONs is changed accordingly to $b_{\mu\nu}(x) \rightarrow b_{\mu\nu}(x) \pm \Delta$, where Δ is not necessarily a multiple of N . For this update, the number of links to be integrated increases with the lattice size. Recall that for the updates discussed previously, the number of links integrated to compute the weights depends only on the type of update and is fixed *a priori* for each of the updates. Although enlarging the size of the space sampled by the algorithm, this nonlocal update might not be enough to guarantee full ergodicity

of the worm algorithm, but it should do more good to ergodicity than not doing any nonlocal update at all. Of course, one can introduce other types of nonlocal updates as, for example, an update of the plaquette occupation numbers attached to a cube. Herein, we will consider only the so-called planar update.

Let us now discuss the group integration to compute the transition probability p . On Fig. 5 we shown the surface over which the plaquette occupation numbers are to be updated. In order to perform the group integration, the links represented by solid lines are set to the identity matrix and those represented by dotted lines are to be integrated exactly for the weight evaluation. In $d > 2$ dimensions and in what respects the group integration, the links on Fig. 5 are coupled with staples in other planes. In the integration to compute the transition probability for this nonlocal update, all those staples are set to be the identity matrix. Again, we are not building a maximal tree but the approximation allows us to get relatively simple expressions in the calculus of the transition probability p .

The local function F_p , associated to the update over a 5×5 plane represented in Fig. 5, contains 24 link variables and is given by

$$F_p = \frac{\text{Tr}[U_1]^{b_1}}{b_1!} \frac{\text{Tr}[U_1^\dagger U_2]^{b_2}}{b_2!} \frac{\text{Tr}[U_2^\dagger U_3]^{b_3}}{b_3!} \times \dots \frac{\text{Tr}[U_{23}^\dagger U_{24}]^{b_{24}}}{b_{24}!} \frac{\text{Tr}[U_{24}]^{b_{25}}}{b_{25}!} \text{Tr}[U_1]^{c_1} \times \text{Tr}[U_2]^{c_2} \text{Tr}[U_3]^{c_3} \dots \text{Tr}[U_{24}]^{c_{24}}, \quad (45)$$

where all b_i are plaquette occupation numbers belonging to the plane where the nonlocal update takes place, the c_i are related to the integrated link U_i and are given by a sum of plaquette occupation numbers belonging to the plaquettes that share U_i in other planes than the updated plane.

Starting the group integration by the link labelled 1 on Fig. 5, the integration function is of the same type as that defined in Eq. (29) and whose solution is given in Eq. (31). The integration leads to a polynomial of the trace of the link with label 2. For the integration of the link labelled 2 one uses the solution in Eq. (31) and repeat the process to the subsequent links, as for the integration of the green and blue paths in the local update associated with Fig. 2.

V. OBSERVABLES

We implement the algorithm to compute the mean value of the plaquette and the mass of the $J^{PC} = 0^{++}$ glueball. The mean value of the plaquette is easily computed in terms of the plaquette occupation numbers. In the partition function given by Eq. (3), the plaquette $U_{\mu\nu}(x)$ comes associated with the factor β . Formally, one can identify a different β with each of the plaquettes

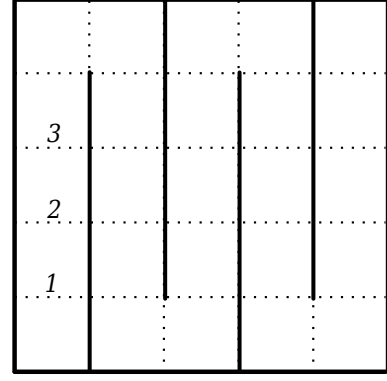


FIG. 5. Two-dimensional representation of the 5×5 lattice with periodic boundary conditions. The solid lines are fixed to the identity and the dotted ones are integrated in the evaluation of the weight function ratio corresponding to a nonlocal plane update.

and make the replacement $\beta \rightarrow \beta_{\mu\nu}(x)$. Ignoring the constant C in Eq. (3), it follows that

$$\frac{\partial \ln Z}{\partial \beta_{\mu\nu}(x)} = \frac{1}{Z} \int \mathcal{D}U \left(\frac{\text{Re Tr}[U_{\mu\nu}(x)]}{N} \right) W[U], \quad (46)$$

$$= \langle N^{-1} \text{Re Tr } U_{\mu\nu}(x) \rangle,$$

where $W[U]$ is the Boltzmann weight factor in the standard representation of the partition function. Performing the same operations with the partition function written in the dual representation, given by Eqs. (8) and (9), it follows that

$$\frac{\partial \ln Z}{\partial \beta_{\mu\nu}(x)} = \frac{1}{Z} \sum_{\{b\}} \left(\frac{b_{\mu\nu}(x)}{\beta} \right) Q_{\{b\}}, \quad (47)$$

and, therefore, the plaquette expectation value is given by the average of the dual variables $b_{\mu\nu}(x)$

$$\left\langle \frac{\text{Re Tr } U_{\mu\nu}(x)}{N} \right\rangle = \left\langle \frac{b_{\mu\nu}(x)}{\beta} \right\rangle. \quad (48)$$

The average of the plaquette expectation value over the lattice volume, called here plaquette mean value u , reads

$$u = \frac{1}{V_p} \left\langle \frac{\sum_{x,\mu\nu} b_{\mu\nu}(x)}{\beta} \right\rangle. \quad (49)$$

The value of u estimated with the worm algorithm will be compared with the output of a conventional Monte Carlo method using heat bath updates.

In this exploratory work besides the mean value of the plaquette we also compute the mass of the scalar glueball with quantum numbers $J^{PC} = 0^{++}$. This requires the building of an interpolation field Φ with the right quantum numbers and writing Φ in terms of the dual variables $b_{\mu\nu}(x)$. A first step toward the computation of the mass

of the scalar glueball is the evaluation of the correlation function

$$G(x - y) = \langle 0 | \Phi(x) \Phi(y) | 0 \rangle. \quad (50)$$

Setting y fixed at the origin of the lattice, then the zero momentum Euclidean space Green's function reads

$$\begin{aligned} G(t) &= \frac{1}{4\pi^2} \int_0^\infty dp \frac{p^2}{\sqrt{p^2 + m^2}} e^{-\sqrt{p^2 + m^2}t} \\ &= \frac{m^2}{4\pi^2} \int_1^\infty dz \sqrt{z^2 - 1} e^{-zmt}, \end{aligned} \quad (51)$$

where m is the mass of the glueball ground state and the last line is the result of making the change of variable $p^2 + m^2 = z^2 m^2$ in the first line. The integration over z is given in terms of the K_1 Bessel:

$$G(t) = \frac{(1/2)!}{2\pi^{5/2}} \frac{m}{t} K_1(mt) \approx \frac{\sqrt{m}}{t^{3/2}} e^{-mt} \left(1 + \mathcal{O}(1/t)\right), \quad (52)$$

where the second expression holds for large values of t .

The lattice version of the operator Φ is constructed by mapping the continuum symmetries and therefore the quantum numbers of the corresponding particle into the hypercubic group [36]. For the ground-state and for the channel $J^{PC} = 0^{++}$, the simplest operator is given by

$$\Phi(t) = \sum_{\vec{x}} \sum_{\substack{\mu < \nu \\ \nu \neq t}} \frac{\text{Re Tr } U_{\mu\nu}(\vec{x}, t)}{N}, \quad (53)$$

i.e., the sum of spacelike plaquettes. With the use of Eq. (48), the operator Φ can be mapped into the dual representation and is given in terms of $b_{\mu\nu}(x)$ as

$$\Phi(t) = \sum_{\vec{x}} \sum_{\substack{\mu < \nu \\ \nu \neq t}} \frac{b_{\mu\nu}(\vec{x}, t)}{\beta}. \quad (54)$$

The estimation of the glueball masses from correlation functions of type given in Eq. (52) with smaller statistical errors is not an easy task. Indeed, given that $G(t)$ decays exponentially with Euclidean time, the signal to noise ratio decreases speedily for large Euclidean time and, therefore, on the lattice one can only rely on a limited number of time slices to estimate m . Although there are a number of techniques to improve the signal to noise ratio, as e.g. the use of anisotropic lattices or the use of smeared operators [32, 34, 35], we will take the interpolating operator as given in Eq. (53), with the representation given in Eq. (54), to test the algorithm.

In practice, for estimating the scalar glueball mass, a number of uncorrelated configurations will be generated and the operator Φ will be computed using Eq. (54). From the interpolating field we evaluate the scalar glueball connected Green function

$$G(t) = \frac{1}{T} \sum_{\tau} [\langle \Phi(t) \Phi(t + \tau) \rangle - \langle \Phi(t) \rangle \langle \Phi(t + \tau) \rangle], \quad (55)$$

where T is the lattice time length and the second term on the right hand side in Eq. (55) removes the vacuum contribution to the signal. The mass of the $J^{PC} = 0^{++}$ glueball is measured fitting the lattice estimation in Eq. (55) to the functional form given in Eq. (52).

VI. RESULTS

In the simulations to be discussed below we start the Markov chain with a cold start, where all $b_{\mu\nu}(x) = 0$, and the Monte Carlo updates use both the local and nonlocal updates. For the local updates a given plaquette occupation number $b_{\mu\nu}(x)$ is chosen randomly and it is proposed to change by ± 2 ; the sign being chosen randomly. This process is repeated V_p times, where V_p is the total number of lattice plaquettes. To this set of updates we call one Monte Carlo step or full sweep for the local update.

For a nonlocal update, a two dimensional surface is chosen randomly on the lattice and for each plaquette occupation number $b_{\mu\nu}(x)$ on the surface a change by ± 1 is proposed randomly. The process is repeated N_p times, where N_p is the number of two dimensional surfaces on the lattice. To this set of updates we call one Monte Carlo step or full sweep for the nonlocal surface update.

A. Sampling and the mean value of the plaquette

For the evaluation of the mean value of the plaquette given in terms of the dual variables, as given in Eq. (49), we simulate two different lattice volumes, 6^4 and 12^4 , for various values of β . For each of the simulations, after discarding 10^3 combined Monte Carlo steps for thermalization, we consider 10^4 configurations separated by 10 combined Monte Carlo steps. Our numerical experiments have shown that a separation of 10 combined Monte Carlo sweeps is enough to decorrelate the observables measured in the current work.

On Fig. 6 we compare the results obtained with our worm algorithm with the results using the standard Wilson action and the heat bath algorithm implemented with the library Chroma [44]. The results shown for the heat bath algorithm refer to simulations performed on a 10^4 lattice, for an ensemble with 10^4 configurations, separated by 5 Monte Carlo steps.

In the top panel of Fig. 6 we show the plaquette mean value obtained in simulations combining the local and nonlocal updates against the results of the standard Wilson action using a heat bath simulation. As can be seen, there is good agreement between the worm algorithm, using any of the local updates, and the heat bath simulation in the strong coupling. The data also suggests that in the weak coupling limit the worm algorithm prediction for u converges to the value given by the heat bath algorithm.

In what concerns the β dependence of the results, the worm algorithm prediction for u starts to deviate from

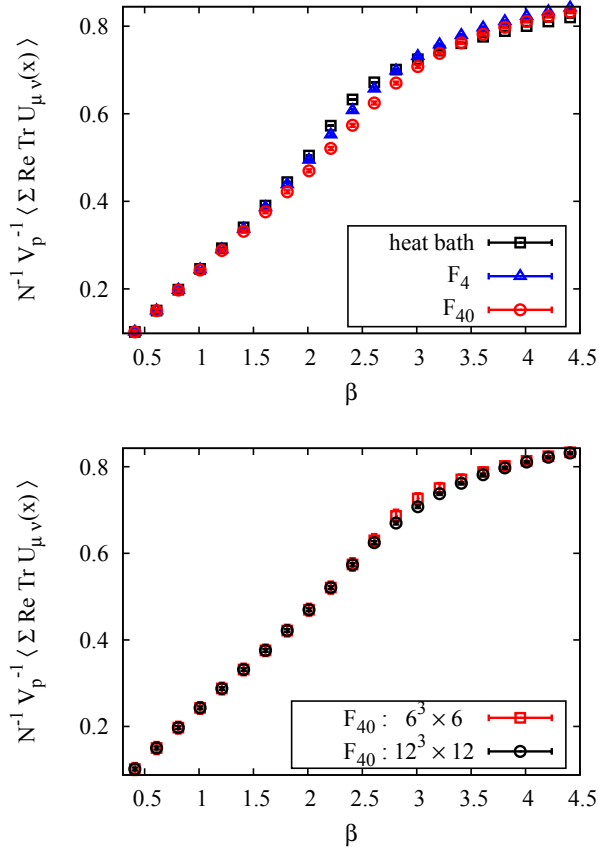


FIG. 6. Mean value of the plaquette from simulations using the heat bath algorithm and the standard Wilson action and the worm algorithm with the dual representation associated with the plaquette occupation numbers. Top panel: Comparison of the performance of the two local updates. Lower panel: Finite volume effects and the worm algorithm.

the heat bath result for $\beta \sim 1.5$ up to $\beta \sim 3$. Its maximal deviation of about 0.1% occurs for $\beta \sim 2.3$. Interestingly, in this range the local algorithm which takes into account the smaller number of integrations, see Sec. IV A 1, is closer to the results of the heat bath simulation. However, as one approaches the continuum limit, i.e. for $\beta \gtrsim 3$, it is the algorithm which uses the other local update, see Sec. IV A 2, which is closer to the heat bath outcome. Indeed, for the algorithm whose local update takes into account the larger number of group integrations the deviations from the heat bath result are marginal for $\beta \gtrsim 3$.

The volume dependence of the worm algorithm is seen in the lower panel of Fig. 6, where the sampling of u is investigated for two different lattice volumes. Recall that the full Monte Carlo update is defined by a combination of local and nonlocal updates. The data show no or only a mild dependence on the lattice volume.

On Fig. 7 we show the relative deviation of the worm algorithm estimation for u with respect to the heat bath results for different lattice volumes. The deviations are negligible in the strong coupling limit and are very small

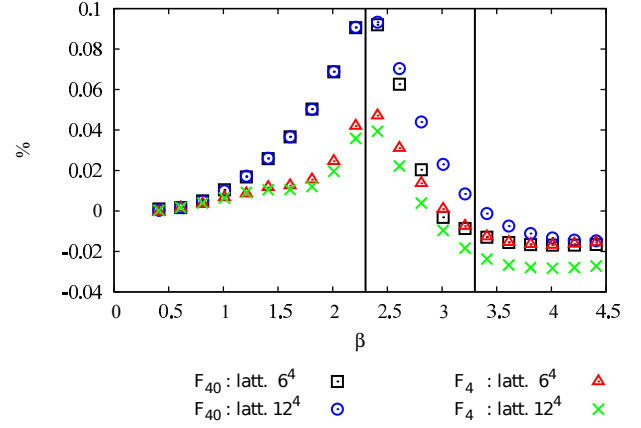


FIG. 7. The same as in Fig. 6 but for the relative deviation of the worm algorithm with respect to the heat bath results. The vertical black lines show the interval of β values where the efficiency of the nonlocal update is higher. See text for details.

when the continuum limit is approached. The maximal deviations $\lesssim 0.1\%$ occur for intermediate values of the coupling around $\beta \sim 2.3$.

The performance of the worm algorithm for different β values and different volumes can be understood looking at the update efficiency \mathcal{E} , defined as its acceptance rate in the Markov chain. As can be seen in the top panel of Fig. 8, the nonlocal update has an essentially vanishing \mathcal{E} , with the exception of the smaller lattice and over a narrow range of β values. Note, however, that the region where the simulations using the two volumes give different values for u , see the lower panel on Fig. 6, is precisely the region of β where the efficiency associated with the nonlocal update has its maximum value. Furthermore, the results of Figs. 6 and 8 suggest that the nonlocal update plays an important role. Indeed, for the smaller lattice volume and for β in the range 2.5–3, the efficiency \mathcal{E} is maximal and non negligible for the nonlocal update, which makes the estimation of u by the worm algorithm closer to the values provided by the heat bath method. The deviations of the worm estimation for u relative to the heat bath result for the smaller volumes are milder for β in the range 2.5–3, as can be seen from Fig. 7. For the larger volumes, \mathcal{E} is always residual and the worm algorithm estimation of u shows larger deviations which are, nonetheless, less than 0.1% relative to the heat bath numbers.

Herein, we considered a single type of nonlocal update but many other possibilities can be explored to achieve a better and more complete sampling of the dynamical range of values allowed for the plaquette occupation number space. Within the rationale considered in this work, the building of a worm algorithm, i.e. the implementation of other types of nonlocal updates, implies a compromise between a given geometrical setting, i.e. the definition of a given set of links over a large region of the lattice, and the ability of being able to perform the

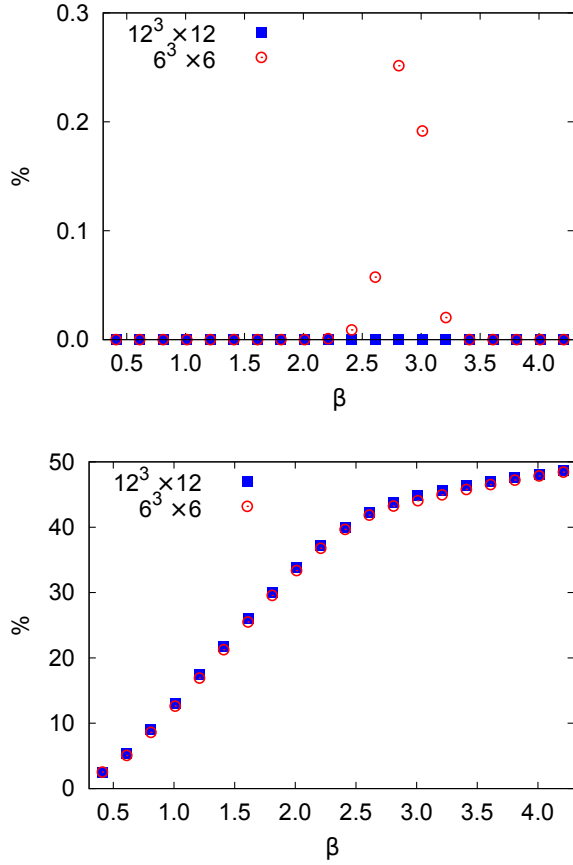


FIG. 8. Worm algorithm efficiency for the various updates. Top panel: Nonlocal update, see Sec. IV B. Bottom panel: Local updates using the function F_{40} , see Sec. IV A 2

group integration over the corresponding sublattices. Recall that, within our framework, the local updates do not sample the entire $\{b\}$ space. For example, for the local updates the $\{b\}$ remain either in the subset of odd or even natural numbers. The nonlocal update were built to allow for a better dynamical range, allowing for transitions in Markov chain where the PONs could become either odd or even natural numbers. The search for other nonlocal type of updates is one of the features that we aim to explore in a future work.

Another way of reading the results in Fig. 8 is that one should improve the efficiency \mathcal{E} of the non local update. Indeed, for the local updates its acceptance rate is always $\sim 10\%$ or above, reaching a value of about 50% as the continuum limit is approached. On the other hand, the nonlocal update defined in Sec. IV B, has an extremely low \mathcal{E} , with has a maximum of $\sim 0.25\%$ for $\beta \sim 2.7$ for the smaller lattice and being always residual for the larger lattice. From the point of view of the worm algorithm, the low values for the efficiency associated with the nonlocal update mean that the plaquette occupation numbers are essentially trapped into the subset of the odd or the even natural numbers which is sampled by the local Monte Carlo updates.

TABLE I. Fits of the glueball correlation function with the reduced chi squared being $\nu^2 = \chi^2/d.o.f.$

Range	Conf. = 1.12357×10^7			Conf. = 1.3259×10^7		
	$m/\sqrt{\sigma}$	g_0	ν^2	$m/\sqrt{\sigma}$	g_0	ν^2
[2:4]	3.62(98)	1.11(54)	0.13	3.62(45)	1.17(61)	0.19
[2:5]	3.61(86)	1.15(48)	0.10	3.62(53)	1.20(54)	0.15
[2:6]	3.61(00)	0.97(91)	0.36	3.61(20)	0.96(99)	0.56

The local updates change, in a single update, a fixed number of $b_{\mu\nu}(x)$ and, in principle, are not so sensitive to volume effects as the nonlocal updates which is affected by surface effects.

B. $J^{PC} = 0^{++}$ glueball mass

For the estimation of the $J^{PC} = 0^{++}$ glueball mass with the worm algorithm we perform simulations with $\beta = 3.01$ on a $10^3 \times 20$ lattice, with a Monte Carlo step combining the local update as defined in Sec. IV A 2 and nonlocal updates as defined in Sec. IV B.

For the conversion into physical units, we rely on Ref. [45] which uses the string tension $\sqrt{\sigma} = 440$ MeV and assumes

$$\ln(\sigma a^2) = -4 \frac{4\pi^2}{\beta_0} \beta + \frac{2\beta_1}{\beta_0^2} \ln\left(\frac{4\pi^2}{\beta_0} \beta\right) + \frac{4\pi^2}{\beta_0} \frac{d}{\beta} + c, \quad (56)$$

where the first two terms are the predictions of 2-loop perturbation theory and the remaining terms parameterize higher-order effects. The parameters $c = 4.38(9)$ and $d = 1.66(4)$ were set by fitting the lattice data for the string tension using simulations with $\beta \in [2.3, 2.85]$. For $\beta = 3.01$, the above relation estimates $a \approx 0.02$ fm for the lattice spacing.

The glueball mass is evaluated from the asymptotic expression for the two-point correlation function

$$G(t) = g_0 \frac{\sqrt{m}}{t^{3/2}} e^{-mt}. \quad (57)$$

Our lattice estimations for $G(t)$ use $\sim 10^7$ configurations and the correlation function can be seen on Fig. 9. Despite using a large ensemble, our Monte Carlo code is not parallelized. However, the ensembles were built running the code on various independent standalone machines. For $t \geq 6$ the lattice two point correlation function becomes negative and compatible with zero within one standard deviation and, therefore, lattice Euclidean times larger than 6 will not be considered.

The correlation function for $t = 1$ does not comply with the remaining values for larger t and with Eq. (57) and, therefore, in the estimation of m it is discarded. In the measurement of the glueball mass we consider three different fitting ranges and two large and independent ensembles as described in Tab. I. For each of the fitting

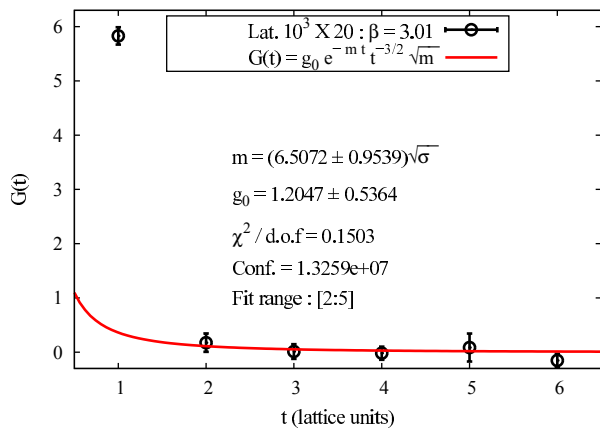


FIG. 9. The lattice estimation correlation function $G(t)$. The curve in red is the fit of the lattice data to the asymptotic expression (57) and for the fitting range $t \in [2, 5]$.

ranges considered, the lattice data are well described by the asymptotic expression for the correlation function in Eq. (57), as can be seen by the values of the $\chi^2/d.o.f.$. Furthermore, m and g_0 are independent of the fitting range. The simulations point towards a glueball mass of 1584 ± 378 MeV for a $\sqrt{\sigma} = 440$ MeV.

The simulation described so far uses a small physical volume and the simplest operator to estimate the $J^{PC} = 0^{++}$ glueball mass. Indeed, none of the available techniques to improve the signal to noise ratio is used in the numerical experiments. However, despite this limitations we are able to reproduce the numbers that can be found in the literature. In Ref. [37] the authors report several estimates for SU(2) scalar glueball mass. Ref. [38] uses the same interpolating operator for the glueball as ours and reports the value $m = (3.7 \pm 1.2) \sqrt{\sigma}$. In Ref. [35], the simulation is done using improved signal to noise methods and the authors report the value $m = (3.12 \pm 0.22) \sqrt{\sigma}$. Finally, the more recent calculation in Ref. [33] gives $m = (3.78 \pm 0.07) \sqrt{\sigma}$. Our estimates for the intermediate fitting range are $m = (3.61 \pm 0.86) \sqrt{\sigma}$ and $m = (3.62 \pm 0.53) \sqrt{\sigma}$, and agree within one standard deviation with the numbers quoted before.

VII. SUMMARY

In the current work we discuss a mapping of the lattice Wilson action into a dual representation, whose dynamical variables, the so-called plaquette occupation numbers $\{b_{\mu\nu}(x)\}$, belong to the natural numbers \mathbb{N}_0 . The partition function of the dual representation of the Yang-Mills theory is given by a sum of weights $Q_{\{U\}}[\{b\}]$, that are functions of the dual variables.

The mapping into the dual representation, i.e. the evaluation of the weights Q , imply an integration of the link variables over the entire lattice volume. In a worm algorithm the transition probability p defining the Markov chain is given by ratios of weights Q . In our proposal the

link integration is simplified in order to get an approximate analytical estimation for p . Indeed, in an update of $b_{\mu\nu}(x)$, the lattice is factorized into a regions containing the plaquette $U_{\mu\nu}(x)$ and the remaining lattice points and a set of links belonging to the interface between the regions is rotated to the identity. In this way, one is able to evaluate exactly and analytically the link integrals which are necessary to estimate the transition probability p .

For the evaluation of the transition probability, the approximations in the link integration are somehow drastic. However, given that the links rotated to the identity are a very small subset of the entire $\{U_{\mu}(x)\}$, one expects that their contribution to p to be subleading. Furthermore, given that the numbers of links set to identity is volume independent, one expects to approximate the exact value of p in the limit of large volumes. Our results for the mean value of the plaquette and the lightest glueball mass show that, even for the small lattices considered herein, the deviations from an exact sampling are indeed small. The worm algorithm discussed herein considers various partitions of the lattice or types of updates that not only improve the ergodicity of the algorithm but also aim to wash out the approximate link integration for the evaluation of p . The different types of updates are named local and nonlocal.

In the class of local updates we consider two different methods which differ in the size of the region containing the link associated with the point where the plaquette occupation number is to be updated. The algorithm also considers a nonlocal update where the link integration is performed exactly over a two dimensional lattice surface where all the associated occupation numbers are to be randomly updated. The nonlocal update improves the ergodicity of the algorithm as it allows to switch the occupation numbers from odd to even and vice-versa, an evolution which is not allowed by the so called local updates.

The simulation results reported use a combination of local updates, with the larger interior integration region, and planar nonlocal updates. The worm algorithm estimates for the plaquette mean value agree well with the corresponding heat bath estimations in the weak coupling limit. In the strong coupling limit the deviation from the heat bath figures seems to be marginal. The worst case scenario occurs at intermediated range of β values, where the deviation relative to the heat bath results is below 0.1%. In what concerns the estimation of the lightest SU(2) glueball mass, the simulations reported here are in good agreement with the literature.

The worm algorithm simulations of the dual representation of SU(2) non-Abelian Yang-Mills theory seems to provide good estimates of non trivial quantities, even though full ergodicity might not have been achieved. The results reported here suggest that the inclusion of larger lattice partitions in the “inner” integral, i.e. including larger numbers of links in the neighbourhood of the updated plaquette occupation number, to estimate the tran-

sition probability takes p closer to its real value. This can be achieved by a careful choice of the “inner” region, i.e. the region which includes the lattice point where the plaquette occupation number is to be updated, and the “outer” sublattices such that one is able to perform necessary group integrals after setting some of the links to the identity. Certainly, any progress in the evaluation of $SU(N)$ integrals, see e.g. Ref. [46], will help in improving the estimation of p . Another possible approach, still to be developed, is the numerical evaluation of the group integrals which, hopefully, could lead to an “exact” estimation of the transition probability.

The algorithm discussed here can be generalized to other gauge groups $SU(N)$ for any number of colors. Another interesting research topic is the inclusion of the fermionic degrees of freedom which, in principle, can be accommodated within the procedure described. These are research problems that we aim to address in the near future.

ACKNOWLEDGMENTS

This research was supported by resources supplied by the Center for Scientific Computing (NCC/GridUNESP) of the São Paulo State University (UNESP) and by resources supplied by the Departament of Physics of Coimbra University. Work partially supported by Fundação de Amparo à Pesquisa do Estado de São Paulo (FAPESP), Grant. No. 2013/01907-0 (G.K.), Conselho Nacional de Desenvolvimento Científico e Tecnológico (CNPq), Grant No. 305894/2009-9 (G.K.), and by CAPES — Brazilian Federal Agency for Support and Evaluation of Graduate Education within the Ministry of Education of Brazil. The authors thank Paulo J. Silva for the heat bath data.

Appendix A: Group integration

Here we will compute some group integrations that appears in the evaluation of the weight function ratio of the non-Abelian gauge partition function written in the dual representation. First we introduce some basic properties of the group integration. Consider a function $f(U)$ where $U \in SU(N)$, as we can see in many textbooks e.g. [1], the group integration is left and right invariant

$$\int dU f(U) = \int dU f(Ug) = \int dU f(g'U) \quad (A1)$$

where g and g' are arbitrary elements of the group $SU(N)$ and the Haar measure are also left and right invariant

$$dU = d(Ug) = d(g'U). \quad (A2)$$

From these basic properties we can conclude

$$\int dU U_{a,b} = 0, \quad (A3)$$

$$\int dU U_{a,b} U_{c,d}^\dagger = \frac{1}{N} \delta_{a,d} \delta_{b,c}, \quad (A4)$$

$$\int dU U_{a_1,b_1} \dots U_{a_k,b_k} \neq 0 \quad \text{If } k \bmod N = 0, \quad (A5)$$

and these properties determine the constraint over the new degrees of freedom discussed in Sec. III.

1. Integration over the green paths

Consider the green path, see Fig. 3, containing the links variables U_{3a}, U_{3b}, U_{3c} and U_{3d} that need be integrated, this path is coupled to the central plaquette (CP) $U_{\mu_0\nu_0}(x_0) = U_1 U_2 U_3 U_4$ by the link U_3 and belong in a plane parallel to CP in the direction ρ . Each link of CP is coupled to one green path, here we will show the integration of the green path coupled to the link U_3 , the precise definition of this green path links are

$$U_{3a} = U_{\nu_0}(x_0 + \hat{\nu}_0 + \hat{\rho} - \hat{\mu}_0), \quad (A6)$$

$$U_{3b} = U_{\mu_0}(x_0 + 2\hat{\nu}_0 + \hat{\rho} - \hat{\mu}_0), \quad (A7)$$

$$U_{3c} = U_{\nu_0}^\dagger(x_0 + \hat{\nu}_0 + \hat{\rho}), \quad (A8)$$

$$U_{3d} = U_{\mu_0}(x_0 + \hat{\nu}_0 + \hat{\rho}), \quad (A9)$$

and the integration in question is given by

$$\begin{aligned} P_{B_G}[U_3] &= \int \widetilde{\mathcal{D}U}_G \text{Tr}[U_3 U_{3d}]^{b_1} \text{Tr}[U_{3c} U_{3d}]^{b_2} \\ &\times \text{Tr}[U_{3a} U_{3b} U_{3c}]^{b_3} \text{Tr}[U_{3a}]^{c_1} \\ &\times \text{Tr}[U_{3b}]^{c_2} \text{Tr}[U_{3c}]^{c_3} \text{Tr}[U_{3d}]^{c_4}. \end{aligned} \quad (A10)$$

The plaquette occupation numbers (PON) b_i are defined as

$$b_1 = b_{\mu_0\rho}(x_0 + \hat{\nu}_0), \quad (A11)$$

$$b_2 = b_{\mu_0\nu_0}(x_0 + \hat{\nu}_0 + \hat{\rho}), \quad (A12)$$

$$b_3 = b_{\mu_0\nu_0}(x_0 + \hat{\nu}_0 + \hat{\rho} - \hat{\mu}_0), \quad (A13)$$

and the collective powers c_i are a sum of PONs and, using Eq. (14), are defined as

$$c_1 = n_{\nu_0}(x_0 + \hat{\nu}_0 + \hat{\rho} - \hat{\mu}_0) - b_3, \quad (A14)$$

$$c_2 = n_{\mu_0}(x_0 + 2\hat{\nu}_0 + \hat{\rho} - \hat{\mu}_0) - b_3, \quad (A15)$$

$$c_3 = n_{\nu_0}(x_0 + \hat{\nu}_0 + \hat{\rho}) - b_3 - b_2, \quad (A16)$$

$$c_4 = n_{\mu_0}(x_0 + \hat{\nu}_0 + \hat{\rho}) - b_2 - b_1. \quad (A17)$$

We use Eq. (31) to solve each integral in the path. Starting the integration by the link U_{3a} we have

$$P_{B_G}[U_3] = \sum_{q_1}^{\min(b_3, c_1)} \Gamma_{q_1}^{b_3, c_1} \int \widetilde{\mathcal{D}U}'_G K_1, \quad (A18)$$

where the coefficients Γ are given by Eq. (32). The function $K_1 = K_1[U_{3b}, U_{3c}, U_{3d}; U_3, \{b'\}]$ is defined by

$$K_1 = \text{Tr}[U_3 U_{3d}]^{b_1} \text{Tr}[U_{3c} U_{3d}]^{b_2} \text{Tr}[U_{3b}]^{c_2} \times \text{Tr}[U_{3c}]^{c_3} \text{Tr}[U_{3d}]^{c_4} \text{Tr}[U_{3b} U_{3c}]^{q_1}, \quad (\text{A19})$$

and the measure $\widetilde{\mathcal{D}}U'_G$ by

$$\widetilde{\mathcal{D}}U'_G = dU_{3b} dU_{3c} dU_{3d}. \quad (\text{A20})$$

Now integrating K_1 with the measure dU_{3b} we find

$$\int \widetilde{\mathcal{D}}U'_G K_1 = \sum_{q_2}^{\min(q_1, c_2)} \Gamma_{q_2}^{q_1, c_2} \int \widetilde{\mathcal{D}}U''_{p1} K_2, \quad (\text{A21})$$

where $K_2 = K_2[U_{3c}, U_{3d}; U_3, \{b'\}]$ and the measure $\widetilde{\mathcal{D}}U''_G$ are defined by

$$K_2 = \text{Tr}[U_3 U_{3d}]^{b_1} \text{Tr}[U_{3c} U_{3d}]^{b_2} \times \text{Tr}[U_{3c}]^{c_3+q_2} \text{Tr}[U_{3d}]^{c_4}, \quad (\text{A22})$$

$$\widetilde{\mathcal{D}}U''_G = dU_{3c} dU_{3d}. \quad (\text{A23})$$

Integrating the link U_{3c} we obtain

$$\int \widetilde{\mathcal{D}}U''_G K_2 = \sum_{q_3}^{\min(b_2, c_3+q_2)} \Gamma_{q_3}^{b_2, c_3+q_2} \int dU_{3d} K_3, \quad (\text{A24})$$

where $K_3 = K_3[U_{3d}; U_3, \{b'\}]$ is defined by

$$K_3 = \text{Tr}[U_3 U_{3d}]^{b_1} \text{Tr}[U_{3d}]^{c_4+q_3}. \quad (\text{A25})$$

Finally integrating the link U_{3d} we have

$$\int dU_{3d} K_3 = \sum_{q_4}^{\min(b_1, c_4+q_3)} \Gamma_{q_4}^{b_1, c_4+q_3} \text{Tr}[U_3]^{q_4}. \quad (\text{A26})$$

Collecting Eqs. (A18), (A21), (A24) and (A26), we have

$$P_{B_G}[U_3] = \sum_{q_1}^{\min(b_3, c_1)} \sum_{q_2}^{\min(q_1, c_2)} \sum_{q_3}^{\min(b_2, c_3+q_2)} \sum_{q_4}^{\min(b_1, c_4+q_3)} \times \Gamma_{q_1}^{b_3, c_1} \Gamma_{q_2}^{q_1, c_2} \Gamma_{q_3}^{b_2, c_3+q_2} \Gamma_{q_4}^{b_1, c_4+q_3} \times \text{Tr}[U_3]^{q_4}, \quad (\text{A27})$$

i.e., a polynomial in $\text{Tr}[U_3]$. This solution can be applied to the other green paths but the definitions of the green path links, the PONs b_i and the sum of PONs c_i change accordingly.

2. Integration over the blue paths

In the Fig. 4 we present the blue path coupled to the link U_3 of CP. Like in the green path case, each link of CP is coupled to one blue path. Here we will show only

the integration of the blue path coupled to the link U_3 , the integration in question is

$$P_{B_B}[U_3] = \int \widetilde{\mathcal{D}}U_B \text{Tr}[\tilde{U}_{3a} \tilde{U}_{3b} \tilde{U}_{3c} \tilde{U}_{3d}]^{\tilde{b}_2} \times \text{Tr}[U_3^\dagger \tilde{U}_{3e} \tilde{U}_{3d}^\dagger]^{\tilde{b}_1} \text{Tr}[\tilde{U}_{3a}]^{\tilde{c}_1} \text{Tr}[\tilde{U}_{3b}]^{\tilde{c}_2} \times \text{Tr}[\tilde{U}_{3c}]^{\tilde{c}_3} \text{Tr}[\tilde{U}_{3d}]^{\tilde{c}_4} \text{Tr}[\tilde{U}_{3e}]^{\tilde{c}_5}, \quad (\text{A28})$$

where the definitions of the blue path links are

$$\tilde{U}_{3a} = U_{\nu_0}(x_0 + 2\hat{\nu}_0 + \hat{\mu}_0), \quad (\text{A29})$$

$$\tilde{U}_{3b} = U_{\mu_0}^\dagger(x_0 + 3\hat{\nu}_0), \quad (\text{A30})$$

$$\tilde{U}_{3c} = U_{\nu_0}^\dagger(x_0 + 2\hat{\nu}_0), \quad (\text{A31})$$

$$\tilde{U}_{3d} = U_{\mu_0}(x_0 + 2\hat{\nu}_0), \quad (\text{A32})$$

$$\tilde{U}_{3e} = U_{\nu_0}(x_0 + \hat{\nu}_0 + \hat{\mu}_0). \quad (\text{A33})$$

The PONs \tilde{b}_i are defined as

$$\tilde{b}_1 = b_{\mu_0\nu_0}(x_0 + \hat{\nu}_0), \quad (\text{A34})$$

$$\tilde{b}_2 = b_{\mu_0\nu_0}(x_0 + 2\hat{\nu}_0), \quad (\text{A35})$$

and the collective powers \tilde{c}_i are defined by

$$\tilde{c}_1 = n_{\nu_0}(x_0 + 2\hat{\nu}_0 + \hat{\mu}_0) - b_2, \quad (\text{A36})$$

$$\tilde{c}_2 = n_{\mu_0}(x_0 + 3\hat{\nu}_0) - b_2, \quad (\text{A37})$$

$$\tilde{c}_3 = n_{\nu_0}(x_0 + 2\hat{\nu}_0) - b_2, \quad (\text{A38})$$

$$\tilde{c}_4 = n_{\mu_0}(x_0 + 2\hat{\nu}_0) - b_2 - b_1, \quad (\text{A39})$$

$$\tilde{c}_5 = n_{\mu_0}(x_0 + \hat{\nu}_0 + \hat{\mu}_0) - b_1. \quad (\text{A40})$$

In order to guarantee that we deal with integration that looks like Eq. (31), we need start the integration by one link of the plaquette $\tilde{U}_{3a}\tilde{U}_{3b}\tilde{U}_{3c}\tilde{U}_{3d}$, here we start by the link \tilde{U}_{3a} , then

$$P_{B_B}[U_3] = \sum_{\tilde{q}_1}^{\min(\tilde{b}_2, \tilde{c}_1)} \Gamma_{\tilde{q}_1}^{\tilde{b}_2, \tilde{c}_1} \int \widetilde{\mathcal{D}}U'_B \tilde{K}_1, \quad (\text{A41})$$

where \tilde{K}_1 and the measure $\widetilde{\mathcal{D}}U'_B$ are defined by

$$\tilde{K}_1 = \text{Tr}[U_3^\dagger \tilde{U}_{3e} \tilde{U}_{3d}^\dagger]^{\tilde{b}_1} \text{Tr}[\tilde{U}_{3b} \tilde{U}_{3c} \tilde{U}_{3d}]^{\tilde{q}_1} \times \text{Tr}[\tilde{U}_{3b}]^{\tilde{c}_2} \text{Tr}[\tilde{U}_{3c}]^{\tilde{c}_3} \text{Tr}[\tilde{U}_{3d}]^{\tilde{c}_4} \text{Tr}[\tilde{U}_{3e}]^{\tilde{c}_5}, \quad (\text{A42})$$

$$\widetilde{\mathcal{D}}U'_B = d\tilde{U}_{3b} d\tilde{U}_{3c} d\tilde{U}_{3d} d\tilde{U}_{3e}. \quad (\text{A43})$$

Now integrating \tilde{K}_1 by the measure $d\tilde{U}_{3b}$ we have

$$\int \widetilde{\mathcal{D}}U'_B \tilde{K}_1 = \sum_{\tilde{q}_2}^{\min(\tilde{q}_1, \tilde{c}_2)} \Gamma_{\tilde{q}_2}^{\tilde{q}_1, \tilde{c}_2} \int \widetilde{\mathcal{D}}U''_B \tilde{K}_2, \quad (\text{A44})$$

where \tilde{K}_2 and the measure $\widetilde{\mathcal{D}U}_B''$ are defined by

$$\begin{aligned} \tilde{K}_2 = & \text{Tr} \left[U_3^\dagger \tilde{U}_{3e} \tilde{U}_{3d}^\dagger \right]^{\tilde{b}_1} \text{Tr} \left[\tilde{U}_{3c} \right]^{\tilde{c}_3} \text{Tr} \left[\tilde{U}_{3d} \right]^{\tilde{c}_4} \\ & \times \text{Tr} \left[\tilde{U}_{3e} \right]^{\tilde{c}_5} \text{Tr} \left[\tilde{U}_{3c} \tilde{U}_{3d} \right]^{\tilde{q}_2}, \end{aligned} \quad (\text{A45})$$

$$\widetilde{\mathcal{D}U}_B'' = d\tilde{U}_{3c} d\tilde{U}_{3d} d\tilde{U}_{3e}. \quad (\text{A46})$$

Integrating the link \tilde{U}_{3c} we obtain

$$\int \widetilde{\mathcal{D}U}_B'' \tilde{K}_2 = \sum_{\tilde{q}_3}^{\min(\tilde{q}_2, \tilde{c}_3)} \Gamma_{\tilde{q}_3}^{\tilde{q}_2, \tilde{c}_3} \int \widetilde{\mathcal{D}U}_B''' \tilde{K}_3, \quad (\text{A47})$$

where \tilde{K}_3 and the measure $\widetilde{\mathcal{D}U}_B'''$ are defined by

$$\begin{aligned} \tilde{K}_3 = & \text{Tr} \left[U_3^\dagger \tilde{U}_{3e} \tilde{U}_{3d}^\dagger \right]^{\tilde{b}_1} \text{Tr} \left[\tilde{U}_{3e} \right]^{\tilde{c}_5} \\ & \times \text{Tr} \left[\tilde{U}_{3d} \right]^{\tilde{c}_4 + \tilde{q}_3}, \end{aligned} \quad (\text{A48})$$

$$\widetilde{\mathcal{D}U}_B''' = d\tilde{U}_{3d} d\tilde{U}_{3e}. \quad (\text{A49})$$

Now integrating the link \tilde{U}_{3d} we can write

$$\int \widetilde{\mathcal{D}U}_B''' \tilde{K}_3 = \sum_{\tilde{q}_4}^{\min(\tilde{b}_1, \tilde{c}_4 + \tilde{q}_3)} \Gamma_{\tilde{q}_4}^{\tilde{b}_1, \tilde{c}_4 + \tilde{q}_3} \int d\tilde{U}_e \tilde{K}_4, \quad (\text{A50})$$

where \tilde{K}_4 is defined by

$$\tilde{K}_4 = \text{Tr} \left[U_3^\dagger \tilde{U}_{3e} \right]^{\tilde{q}_4} \text{Tr} \left[\tilde{U}_{3e} \right]^{\tilde{c}_5}. \quad (\text{A51})$$

Finally, integrating the link \tilde{U}_{3e} we have

$$\int d\tilde{U}_e \tilde{K}_4 = \sum_{\tilde{q}_5}^{\min(\tilde{q}_4, \tilde{c}_5)} \Gamma_{\tilde{q}_5}^{\tilde{q}_4, \tilde{c}_5} \text{Tr} [U]^{\tilde{q}_5}. \quad (\text{A52})$$

Inserting Eqs. (A44), (A47), (A50) and (A52) into Eq. (A41) we can write

$$\begin{aligned} P_{\mathcal{B}_B}[U_3] = & \sum_{\tilde{q}_1}^{\min(\tilde{b}_2, \tilde{c}_1)} \sum_{\tilde{q}_2}^{\min(\tilde{q}_1, \tilde{c}_2)} \sum_{\tilde{q}_3}^{\min(\tilde{q}_2, \tilde{c}_3)} \sum_{\tilde{q}_4}^{\min(\tilde{b}_1, \tilde{c}_4 + \tilde{q}_3)} \\ & \times \sum_{\tilde{q}_5}^{\min(\tilde{q}_4, \tilde{c}_5)} \Gamma_{\tilde{q}_1}^{\tilde{b}_2, \tilde{c}_1} \Gamma_{\tilde{q}_2}^{\tilde{q}_1, \tilde{c}_2} \Gamma_{\tilde{q}_3}^{\tilde{q}_2, \tilde{c}_3} \Gamma_{\tilde{q}_4}^{\tilde{b}_1, \tilde{c}_4 + \tilde{q}_3} \\ & \times \Gamma_{\tilde{q}_5}^{\tilde{q}_4, \tilde{c}_5} \text{Tr} [U_3]^{\tilde{q}_5}. \end{aligned} \quad (\text{A53})$$

As in the green path case, the outcome is a polynomial. The above solution can be used to evaluate all blue path integrations but we need to be careful, the definitions of the blue path links, the PONs b_i and the sum of PONs c_i change accordingly.

-
- [1] C. Gattringer and C. B. Lang, *Quantum Chromodynamics on the lattice: An Introductory Presentation* (Springer, 2010).
 - [2] K. Splittorff and B. Svetitsky, Phys. Rev. **D75**, 114504 (2007).
 - [3] K. Splittorff and J. J. M. Verbaarschot, Phys. Rev. **D75**, 116003 (2007).
 - [4] C. Gattringer and K. Langfeld, Int. J. Mod. Phys. **A31**, 1643007 (2016).
 - [5] G. Aarts, Pramana **84**, 787 (2015).
 - [6] P. de Forcrand, J. Langelage, O. Philipsen, and W. Unger, Phys. Rev. Lett. **113**, 152002 (2014).
 - [7] P. de Forcrand and M. Fromm, Phys. Rev. Lett. **104**, 112005 (2010).
 - [8] P. Rossi and U. Wolff, Nucl. Phys. **B248**, 105 (1984).
 - [9] N. Prokof'ev and B. Svistunov, Phys. Rev. Lett. **87**, 160601 (2001).
 - [10] T. A. DeGrand and C. E. DeTar, Nucl. Phys. **B225**, 590 (1983).
 - [11] Y. Delgado Mercado, H. G. Evertz, and C. Gattringer, Phys. Rev. Lett. **106**, 222001 (2011).
 - [12] U. Wolff, Nucl. Phys. **B824**, 254 (2010).
 - [13] U. Wolff, Nucl. Phys. **B832**, 520 (2010).
 - [14] F. Bruckmann, C. Gattringer, T. Kloiber, and T. Sulejmanpasic, Phys. Lett. **B749**, 495 (2015).
 - [15] A. H. Castro Neto, F. Guinea, N. M. R. Peres, K. S. Novoselov, and A. K. Geim, Rev. Mod. Phys. **81**, 109 (2009).
 - [16] V. Ayyar and S. Chandrasekharan, Phys. Rev. **D91**, 065035 (2015).
 - [17] S. Chandrasekharan, Eur. Phys. J. **A49**, 90 (2013).
 - [18] S. Chandrasekharan and A. Li, Phys. Rev. **D88**, 021701 (2013).
 - [19] S. Chandrasekharan and A. Li, Phys. Rev. Lett. **108**, 140404 (2012).
 - [20] M. Fromm, J. Langelage, S. Lottini, and O. Philipsen, JHEP **01**, 042 (2012).
 - [21] C. Gattringer and T. Kloiber, Nucl. Phys. **B869**, 56 (2013).
 - [22] T. Korzec, I. Vierhaus, and U. Wolff, Comput. Phys. Commun. **182**, 1477 (2011).
 - [23] C. Gattringer and T. Kloiber, Phys. Lett. **B720**, 210 (2013).
 - [24] M. G. Endres, Phys. Rev. **D75**, 065012 (2007).
 - [25] T. Rindlisbacher, O. Åkerlund, and P. de Forcrand, Nucl. Phys. **B909**, 542 (2016).
 - [26] M. Panero, JHEP **05**, 066 (2005).
 - [27] V. Azcoiti, E. Follana, A. Vaquero, and G. Di Carlo, JHEP **08**, 008 (2009).
 - [28] Y. Delgado Mercado, C. Gattringer, and A. Schmidt, Phys. Rev. Lett. **111**, 141601 (2013).
 - [29] Y. Delgado Mercado, C. Gattringer, and A. Schmidt, Comput. Phys. Commun. **184**, 1535 (2013).
 - [30] D. H. Adams and S. Chandrasekharan, Nucl. Phys. **B662**, 220 (2003).
 - [31] C. Gattringer and C. Marchis, Nuclear Physics B **916**, 627 (2017).
 - [32] Y. Chen *et al.*, Phys. Rev. **D73**, 014516 (2006).
 - [33] B. Lucini, M. Teper, and U. Wenger, JHEP **06**, 012 (2004).

- [34] M. Albanese *et al.* (APE), Phys. Lett. **B192**, 163 (1987).
- [35] M. Teper, Phys. Lett. **B183**, 345 (1987).
- [36] B. Berg and A. Billoire, Nucl. Phys. **B221**, 109 (1983).
- [37] M. Falcioni, E. Marinari, M. L. Paciello, G. Parisi, B. Taglienti, and Y.-c. Zhang, Nucl. Phys. **B215**, 265 (1983).
- [38] B. Berg, Phys. Lett. **B97**, 401 (1980).
- [39] F. BrÄEnner and A. Rebhan, Phys. Rev. Lett. **115**, 131601 (2015).
- [40] K. G. Wilson, Phys. Rev. **D10**, 2445 (1974).
- [41] M. Newman and G. Barkema, *Monte Carlo Methods in Statistical Physics* (Clarendon Press, 1999).
- [42] M. J. Creutz, *Quarks, Gluons and Lattices* (Cambridge University Press, 1985).
- [43] K. E. Eriksson, N. Svartholm, and B. S. Skagerstam, J. Math. Phys. **22**, 2276 (1981).
- [44] R. G. Edwards and B. Joo (SciDAC, LHPC, UKQCD), Nucl. Phys. Proc. Suppl. **140**, 832 (2005).
- [45] J. C. R. Bloch, A. Cucchieri, K. Langfeld, and T. Mendes, Nucl. Phys. **B687**, 76 (2004).
- [46] J.-B. Zuber, J. Phys. **A50**, 015203 (2017).